NEUTRON-RICH NUCLEOSYNTHESIS IN CARBON DEFLAGRATION SUPERNOVAE

S.E. Woosley[1]

Max Planck Institut für Astrophysik, Karl Schwarzschild Str.1, 85740 Garching, Germany

ABSTRACT

Accreting carbon-oxygen white dwarfs approaching the Chandrasekhar Mass may provide a substantial fraction of Type Ia supernovae. The hydrodynamics of nuclear burning in these models remains uncertain, but all current models are characterized by an initial period of slow, nearly laminar flame propagation at a well known conductive speed. For cold white dwarfs and slow accretion, the density at the center of the white dwarf at ignition may be quite high, extending perhaps beyond the highest value allowed before accretion induced collapse occurs, $\sim 9 \times 10^9$ g cm^{-3}. The nucleosynthesis that occurs in stars slightly below this critical value, specifically $\rho_c = 2$ to 8×10^9 g cm^{-3}, is explored here using a large nuclear reaction network that allows the resulting abundances of neutron-rich nuclei in the mass range 12 to 90 to be accurately determined for realistic models of the explosion. It is found that these explosions are responsible for producing the solar abundances of ^{48}Ca, ^{50}Ti, ^{54}Cr, and ^{70}Zn, with appreciable contributions to ^{58}Fe, ^{64}Ni, ^{66}Zn, ^{76}Ge, ^{82}Se, and the gamma-astronomy candidate, ^{60}Fe. Provided a prompt detonation does not occur, these results are insensitive to the physics of flame propagation after the first few hundredths of a solar mass has burned. They are, however, mildly sensitive to the ignition density and uncertain weak interaction rates below $Y_e \approx 0.42$. Since these nuclei, especially ^{48}Ca, cannot be produced anywhere else in nature, the results show that Chandrasekhar Mass explosions must occasionally occur (an event rate about 2% of the observed Type Ia supernova rate is estimated for these higher density explosions), however most Type Ia supernova must ignite at an appreciably lower density, 2×10^9 g cm^{-3}. Implications for gamma-ray astronomy and meteorite anomalies are briefly discussed.

Subject headings: nucleosynthesis – stars: supernovae: Type Ia

[1]permanent address: Board of Studies in Astronomy and Astrophysics, University of California, Santa Cruz, CA 95064

1. INTRODUCTION

The mechanism whereby an accreting carbon-oxygen white dwarf explodes as a Type Ia supernova continues to be uncertain, but there are compelling reasons to think that a portion, perhaps most of these events, are dwarfs that have approached the Chandrasekhar Mass, $M_{\rm Chand} \approx 1.39\ M_\odot$. These reasons include: 1) the recent identification of supersoft x-ray sources (Rappaport, DiStefano, & Smith 1994) as the possible progenitors; 2) good agreement of the prototypical $M_{\rm Chand}$ model, W7 (Nomoto, Thielemann & Yokoi 1984) with the observed spectra of typical Type Ia supernovae; 3) the good agreement of light curves from this class of model with a variety of Type Ia supernovae (Höflich & Khokhlov 1996); and 4) the present difficulty achieving a robust explosion in three-dimensional sub-$M_{\rm Chand}$ models (Benz 1996, Garcia-Senz, Bravo, & Woosley 1996).

If the ignition density in the typical Type Ia model is too high, unacceptable nucleosynthesis results (Woosley & Weaver 1986). It is currently thought that the ignition density for a common Type Ia supernova model must be $\lesssim 1.5 \times 10^9$ g cm^{-3} (Nomoto, Iwamoto, & Thielemann 1996;Thielemann et al. 1996). A similar, but slightly larger value is found in the present paper. This would require quite rapid accretion at nearly the Eddington value.

Less frequently, a cold white dwarf, typically one accreting at a lower rate, may also grow to $M_{\rm Chand}$ and ignite at a higher density (Canal, Isern, & Labay 1990, Nomoto & Kondo 1991, Hernanz & Isern 1992). Several independent calculations (Timmes & Woosley 1992, Isern & Canal 1994, Garcia-Senz 1992, Woosley & Eastman 1992) give a critical ignition density, providing prompt detonation does not occur, around 9×10^9 g cm^{-3}. Above this density, nuclear burning will initiate collapse, not explosion. Between the cases of accretion induced collapse and normal Type Ia supernovae, there should be white dwarfs that ignite at intermediate density and explode. It is the nucleosynthesis in these supernovae, especially those igniting around 4 to 8×10^9 g cm^{-3}, that will be explored here. The reason for a bifurcation between ignition below 2×10^9 g cm^{-3} and significantly above is not clear at the present time but may involve both the accretion rate and metallicity. The operation of the URCA process (Iben 1982, Barkat & Wheeler 1990, Aparicio & Isern 1993) may be important in delaying ignition to high density for a portion of the explosions.

Generically, we are interested in matter that achieves nuclear statistical equilibrium and then experiences electron capture for a period of about 1 s at the ignition density. For the densities considered, this will give central electron mole numbers, $Y_{ec} \approx 0.41$. Under these conditions, it is known (Hartmann, Woosley, & El Eid 1985, Aufderheide et al. 1994, Meyer, Krishnan, & Clayton 1996) that neutron-rich species, especially ^{48}Ca with its closed neutron (28) and proton (20) shells, are quite abundant. As Meyer et al. have emphasized, the low entropy freeze-out of this matter enhances the ^{48}Ca abundance even more.

These conditions cannot be achieved in Type II and Ib supernovae. While the requisite values of Y_e exist in the ejecta just outside the neutron star (Woosley et al. 1994), the mass is small and, more importantly, the entropy is so high (as is necessary to guarantee ejection from the higher gravitational potential) that the freeze-out will be alpha-rich. This leads to the production of nuclei well above the iron group, and in the extreme case, the r-process (Woosley & Hoffman 1992), not ^{48}Ca.

That neutron-rich nucleosynthesis, especially the production of ^{54}Cr, would occur in the central regions of carbon-deflagration supernovae was first pointed out by Woosley & Weaver (1986; 1994). Preliminary estimates of the ^{48}Ca, ^{50}Ti, and ^{54}Cr yields for representative models were given by Woosley & Eastman (1992) and Woosley, Weaver, & Hoffman (1995). Here the nucleosynthesis is calculated using a much larger reaction network in several white dwarfs exploding from a higher density than considered by Woosley & Eastman (1992) and details of the calculation are presented.

Section 2 discusses the physics employed in the calculation and the stellar model. Section 3 gives the results and discusses their implications, and section 4, a few conclusions.

2. PHYSICS OF THE CALCULATION

2.1. Nuclear reaction network

The two nuclear reaction networks employed in this study are given in Table 1. The 421 isotope network was used for ignition densities below $\rho_9 = \rho/10^9$ g cm^{-3} = 6; the larger 442 isotope network was used at higher densities. Each isotope listed is connected to the others by all accessible charged particle and photon induced interactions involving a single neutron, proton, or $\alpha-$particle in an entrance or exit channel, and the heavy ion reactions, 3α, $^{12}C+^{12}C$, $^{12}C+^{16}O$, and $^{16}O+^{16}O$. In addition, all important weak interactions are included for nuclei with A less than 60. The reaction rates are the same as those employed in Woosley & Hoffman (1992) and are taken mostly from Caughlan & Fowler (1988); Woosley et al. (1978); and Fuller, Fowler, & Newman (1980, 1982, 1985) with additional unpublished rates calculated by Hoffman (private communication). The weak rates of Fuller et al. used here include beta decay as well as electron capture and positron emission. Only ground state weak rates were used for nuclei heavier than A = 60. A tabulation of all rates used is available.

The major deficiency in the nuclear data is the lack of reliable weak interaction rates above mass 60. Aufderheide et al. (1994) have shown that for $Y_e \lesssim 0.42$ in nuclear statistical equilibrium, the dominant weak rates shift to nuclei well above the iron group, nuclei for which no weak interaction rates were available for the present calculation. Approximate beta equilibrium is achieved here, and the most neutron-rich zone studied has $Y_e = 0.40$. The most interesting nucleosynthesis occurs in zones having $Y_e = 0.41$ to 0.42. It is likely that using a more complete set of weak interactions would only affect the rate at which the steady value of Y_e is achieved, but not the value in ejected material. However, in the future when additional weak rates are available in a form easily used by the machine, calculations should be repeated for the higher density models.

Different nuclear reaction networks were used in the nucleosynthesis study and for energy generation in the stellar code. The stellar code uses a 19 isotope approximation network in regions where oxygen still exists ($X(^{16}O)$ greater than 0.04) and a 135 isotope quasi-equilibrium network at higher temperatures for silicon burning and beyond (Weaver, Zimmerman, & Woosley 1978). This quasi-equilibrium code also uses the weak rates of Fuller et al. below A = 60. The large nucleosynthesis network (Table 1) was only updated in zones where the temperature or density were changing (2% and 5% limits per cycle respectively), but a nuclear update was forced to occur in every zone every 100 cycles. A typical explosion calculation generated 35,000 models. Both the energy generation and and Y_e agreed between the stellar network and the nucleosynthesis network at all times.

Mass conservation can become a problem in nuclear reaction networks that stay at high temperature in equilibrium for a long time. The worst mass conservation was in the central zone, typically 0.03%. This was not deemed to be a problem.

2.2. The stellar models

A white dwarf having a composition of 50% each carbon and oxygen (no heavier elements and, therefore, no neutron excess) and a mass 1.30 $M_\odot$ was generated in hydrostatic equilibrium, but not thermal equilibrium using the implicit 1-D hydrodynamics code, KEPLER (Weaver, Zimmerman, & Woosley 1978). This initial model had a central temperature of 10^8 K. No single carbon-oxygen dwarf of such great mass is expected to exist in nature, but since we are only interested in the explosive evolution, the computational convenience of a constant composition suffices. The dwarf was allowed to cool for 30 Myr until thermal equilibrium was reached and its luminosity had declined to 0.1 $L_\odot$. This corresponded to a central temperature of 2.1×10^7 K and a density of 5.6×10^8 g cm^{-3}. Accretion was then simulated by increasing the surface boundary pressure and adding LaGrangian mass shells of 0.01 $M_\odot$ at appropriate intervals until a nuclear runaway began in the stellar center. Neutrino losses played no role in this runaway. Nuclear reactions accelerated when nuclear energy generation greatly surpassed the luminosity that had been carried by conduction. The ignition density was therefore sensitive to the accretion rate. For a typical model (later to be NCD6A), ignition occurred at a temperature of about 1.5×10^8 K and a density, $\rho_9 = \rho/10^9$ g cm^{-3} = 6.3. At this point the mass of the white dwarf was 1.39 $M_\odot$ and the radius, 1.5×10^8 cm. Over the next 10,000 years, convection transported energy from nuclear burning as the central temperature rose and the density declined. When the central temperature equaled 7×10^8 K, convection was turned off as the nuclear and convection time scales had become equal. Further (artificial) maintenance of an adiabatic temperature gradient in such a finely zoned model leads to a prompt detonation (Woosley 1990). Once convection was halted the temperature rose very rapidly and a localized flame developed in the central zone.

The zoning in the central regions, where the nucleosynthesis will be of greatest interest, was very fine in all models. The central zone had 5×10^{-5} $M_\odot$ and there were 31 zones of logarithmically increasing mass inside of the first 0.01 $M_\odot$ of the white dwarf. The entire model at the time of runaway had 180 zones. By the time the runaway became localized the density in the center had declined to $\rho_9 = 5.8$. This is the starting point for the real calculation and defines Model NCD6 (Neutron-rich Carbon Deflagration starting at a peak central density, ρ_9, near 6). Four other similar models were prepared in which the central densities at the time the flame first formed and started to propagate were $\rho_9 = 2.0$ (Model NCD2), 4.0 (Model NCD4), 7.5 (Model NCD7), and 8.2 (Model NCD8). We will follow Model NCD6 in some detail, but give the nucleosynthesis from the others for comparison.

Interesting behavior was observed in Model NCD8 near ignition. If convection was left on until the central temperature reached 7×10^8 K, as in the other three models, the star promptly detonated. This is due to the smaller critical mass for detonation (Woosley 1990, Blinnikov & Khokhlov 1987) at the higher density and a shallower temperature gradient. The nucleosynthesis from this model, NCD8D, was computed for comparison with the others. A second model, NCD8, identically derived, but with convection halted at $T_c = 5 \times 10^8$ K, burned as a deflagration. Electron capture reduced Y_e in this model rapidly behind the burning front so that the density rose (in the central regions) to its pre-burning value only 30 km behind the flame. This severely limited the range of Rayleigh-Taylor unstable wavelengths and the flame speed remained near the laminar value for some time. As a result, this model nearly collapsed, the central density briefly rising before burning farther out in the star led to expansion and explosion. It is felt that Model(s) NCD8 represent the extreme of high density expected in this sort of supernova. A slightly higher ignition density would have led to collapse. Similar NCD8D represents the most rapid possible expansion from this high density state - a prompt detonation. As we shall see, its nucleosynthesis was quite different.

In reality, the propagation of a subsonic flame beyond the stable laminar stage involves very complex physics that can only be approximated in a multi-dimensional calculation (Khokhlov 1995, Niemeyer & Woosley 1996). However, it will turn out that the nucleosynthesis of greatest interest occurs in the first 0.02 $M_\odot$ that burns. Except for the Landau-Darrieus instability, which is known to have only a minor effect at such high density (Blinnikov & Sasorov 1995), one expects that multi-dimensional aspects of the problem (especially the Rayleigh-Taylor and Kelvin-Helmholtz instabilities) will not manifest themselves at such early times. Prior to the development of these instabilities, turbulence will exist only at a low level, essentially given only by the pre-runaway convection. Thus it is reasonable to propagate the flame using a fractal prescription that accounts for a mild amount of surface deformation. Consequently, the flame propagates through the first 0.02 $M_\odot$ at essentially the laminar speed (Timmes & Woosley 1992).

One may also be concerned as to whether the flame will actually ignite at the center of the star (Garcia-Senz & Woosley 1995). Presumably it will not, but the density of the white dwarf 100 km out from the center is only $\sim$10% less than the central density. Since we explore a range of a factor of four in central density here anyway, nucleosynthesis in a model ignited off center may be thought of as an uncertain recalibration of the central density at which the runaway occurs. The key point is that burning 0.02 $M_\odot$ of the white dwarf causes very little expansion of the star, no matter where it is burned (despite the proximity of the structural adiabatic index to 4/3).

The prescription used to describe flame propagation beyond the laminar phase is based upon Timmes (1994) and Woosley (1990). The speed of the burnt surface in a frame co-moving with the flame (LaGrangian co-ordinate) is

$$v_{\text{flame}} \;=\; \text{Max}(v_{\text{cond}}, v_{\text{eff}})$$

where v_{cond} is the laminar flame speed given as a function of density and composition by Timmes & Woosley (1992). The conductive speed is obtained by interpolation in tables rather that the relatively inaccurate fitting formula given by Timmes and Woosley. For the composition employed and densities, $\rho_9 = 2$, 4, 6, and 8, v_{cond} is 76, 143, 214, and 256 km s^{-1}.

The *effective* flame speed,v_{eff}, is given by its distorted surface area in a fractal geometry having dimension as a function of time

$$D_{\text{eff}} \;=\; D_{\max} \;-\; (D_{\max} - 2)(\frac{\lambda_{\min}}{\lambda_{\max}})^{2/3}$$

where $\lambda_{\min}$ and $\lambda_{\max}$ are the minimum and maximum wavelengths to which the fractal description applies. Prescriptions for these wavelengths are given by Timmes & Woosley. In particular, the maximum unstable wavelength is limited, not only by the size of the region that has burned, but by electron capture which restores the density inversion developed in the flame. That is

$$\lambda_{\max} \;=\; \text{Min}(r_b, v_{\text{cond}} t_{\text{rec}})$$

with r_b the radius of the burned out region and $t_{\rm rec}$ is the time it takes for electron capture to restore the density behind the flame to its value ahead of the flame. This condition is important at early times in the high density flames considered here. For a time they are stabilized by electron capture. No multipliers were applied to these time-dependent wavelength ranges. They are as defined in Timmes & Woosley (1992).

The explosion characteristics of a model are then specified by its ignition density, composition, and a choice of the limiting fractal dimension. Here two values of $D_{\rm max}$ = 2.45 and 2.55 were employed for each model. Thus Model NCD4A ignites at a central density of 4.0×10^9 g cm^{-3} and experiences a parameterized explosion with $D_{\rm max} = 2.45$. Model NCD4B is identical, except $D_{\rm max} = 2.55$. There is no compelling physical basis for these choices other than the fact that they lead to the burning of fractions of the white dwarf that probably bound what is acceptable for Type Ia supernovae, (∼50% to 100% mass consumption; Fig. 1; Table 2). It is noteworthy, however, that the intermediate value $D_{\rm max} = 2.50$ would give an effective speed independent of the conductive speed and equal here to

$$v_{\rm eff} \;=\; (\frac{g_{\rm eff}}{8\pi})\,t,$$

where $g_{\rm eff}$ is $GM(r)/r^2$ multiplied by the change in density across the burning front divided by the density. This is the same dependence on time, and approximately the same proportionality constant as the Sharp-Wheeler model (Sharp 1984) for an ensemble of buoyant bubbles resulting from a non-linear Rayleigh-Taylor instability. The Sharp-Wheeler Model gives $v_{\rm eff} \;=\; 0.10 g_{\rm eff} t$.

Despite the care taken to provide a reasonable description of the flame propagation throughout the star, the nucleosynthesis of greatest interest for these models exploding from high density is determined during the first 0.02 $M_\odot$. During that period the flame speed is essentially given by the well determined (laminar) conductive value. What is most important then is the ignition density and the expansion time scale.

3. RESULTS

3.1. Model explosions

Moving to the time-dependent development of a typical model, it took Model NCD6A 0.50 s to burn the first 0.03 $M_\odot$, a distance of 150 km. By this point Y_e in the center had fallen, as a result of electron capture, to 0.412. The central density at this point was $\rho_9 = 5.4$, and the density at the flame, $\rho_9 = 4.6$. After a total of 0.84 s, 0.25 $M_\odot$ had burned (flame at 450 km partly due to expansion) and the central density and Y_e had fallen to $\rho_9 = 2.3$ and 0.408. Y_e later rose slightly to 0.414 in response to beta decay as the density declined.

At the end of the explosion (the last calculation was at 10 seconds in all cases), Model NCD6A had a kinetic energy at infinity of 7.7×10^{50} erg and a composition rich in iron group nuclei. The ^{56}Ni abundance ejected was 0.39 $M_\odot$, but there were 0.31 $M_\odot$ of other iron group elements.

For comparison, Model NCD6B took 0.48 s to burn the first 0.03 $M_\odot$, also 150 km, at which point Y_e in the center was 0.413 and the density $\rho_9 = 5.5$. It took 0.72 s to burn 0.26 $M_\odot$ at which time the central value of Y_e was 0.409. The final kinetic energy for NCD6B was 1.8×10^{51} erg and the mass of ^{56}Ni synthesized, 0.88 $M_\odot$. Almost no carbon or oxygen was left unburned in this or any of the "B" model explosions.

Properties of the other models are summarized in Table 2.

3.2. Nucleosynthesis

Tables 3, 4 and 5 give the details of the nucleosynthesis from the 11 calculations. Table 3 gives the masses of abundant nuclei ejected in only the inner 0.03 $M_\odot$. These might be of interest to people seeking correlated isotopic abundance anomalies in meteorites (§4). Table 4 gives the ratio of the the *total* mass ejected by each model in the form of each isotope (after all radioactivities have decayed) compared to the sun (Anders & Grevesse 1989) and normalized to unit production of iron. The many numbers larger than unity in Table 4 for all models denser than NCD2 show that these sorts of supernovae, even the relatively low density Model NCD4A, cannot be the source of a major fraction of iron in nature. If they produced ^{56}Fe in the sun, they would overproduce other isotopes by the indicated factors. However, based solely upon their nucleosynthesis, Models NCD2A and, especially, NCD2B would be acceptable as typical Type Ia supernovae. Timmes, Woosley, & Weaver (1995a) find that 1/3 to 2/3 of ^{56}Fe is made in Type Ia's and the massive stars are somewhat deficient in the species that have factors bigger than 1 in Table 4 for NCD2B. Note that all the models studied here had an initial metallicity of zero and thus would correspond most closely to Pop II, the probable progenitors of Type Ia supernovae. Higher metallicities would have led to increased production of ^{54}Fe and ^{58}Fe in Models NCD2.

We conclude that 2×10^9 g cm^{-3} is the *maximum* ignition density that can be tolerated in the standard Type Ia model. All the other models make excessive amounts of neutron-rich species and must be rare.

For those interested in detail, or use of the results for Galactic chemical evolution studies, Table 5 gives the masses of each isotope (after all radioactivities have decayed) ejected by each model in solar masses. A few interesting long-lived radioactivities are also given.

It is helpful in understanding the productions in the tables to examine at abundances in nuclear statistical equilibrium (e.g., Aufderheide et al. 1994; their Fig 1) as a function of $Y_e = (1-\eta)/2$, with η, the neutron excess. In general, a nucleus is most abundant at a a value of Y_e characterizing its own structure, $Y_e = Z/A$. Closed shell structures also influence the abundances considerably. Thus ^{48}Ca is made as itself for Y_e in the range 0.41 to 0.42, its double magic shell structure (Z = 20, N = 28) affording a special degree of stability in equilibrium. ^{50}Ti is also abundant at $Y_e \approx 0.42$ because of the closed neutron shell at N = 28. ^{54}Cr is made as itself for $Y_e \approx 0.44$ to 0.45. ^{66}Zn and ^{70}Zn are produced as the radioactive progenitors ^{66}Ni and ^{70}Ni which are major constituents at Y_e = 0.42 and 0.40 respectively because of their closed (Z = 28) proton shell. ^{76}Ge is made as ^{76}Zn for $Y_e \approx 0.40$. ^{82}Se is made as ^{82}Ge, also for $Y_e \approx 0.40$ (and less) because of the closed shell at N = 50.

In retrospect, the network (Table 1), which seemed so large when the study was begun, should have had a few more neutron-rich isotopes in the vicinity of Ge and Zn because ^{76}Zn and ^{82}Ge at its edge. Probably this makes little difference because ^{76}Zn and ^{82}Ge are predicted to have large abundances for $Y_e = 0.40$ in nuclear statistical equilibrium (Aufderheide et al. 1994). The value of Y_e is more critical and is uncertain for Models NCD8, and maybe NCD7, owing to lack of weak rates above A = 60. It is expected that the results for these models are qualitatively correct, but perhaps inexact.

^{84}Kr is made as ^{84}Se whose abundance is appreciable at $Y_e \approx 0.41$ again because of its N= 50 neutron shell.

Several long lived ($\gtrsim 10^6$ y) radioactivities are given at the end of Table 2. Of special interest is ^{60}Fe.

4. DISCUSSION AND CONCLUSIONS

As Table 4 shows, it is possible to make the solar abundances of ^{48}Ca, ^{50}Ti, ^{54}Cr, and probably ^{70}Zn in exploding white dwarfs that ignite at densities $\gtrsim 5 \times 10^9$ g cm^{-3}. The synthesis of these nuclei is not sensitive to the uncertain flame physics so long as a prompt detonation does not occur. Tables 4A and 4B bracket the nucleosynthesis expected for any realistic model. The production of ^{70}Zn is less accurately calculated than the other three because of inadequacies in the network and weak rates employed at $Y_e \approx 0.40$, but appreciable synthesis of this isotope is also assured.

Given that these four isotopes, especially ^{48}Ca, cannot be produced anywhere else in nature, several conclusions emerge. First, this kind of event must occasionally happen. That white dwarfs can grow to this mass and explode is encouraging to attempts to make common Type Ia supernovae by a similar evolutionary path, but igniting at a lower density. An ignition density for the common event of $\rho_9 \lesssim 2.0$ is estimated here (see also Woosley & Weaver 1986 and Nomoto, Iwamoto, & Thielemann 1996). However, since the supernovae that make ^{48}Ca, etc. are rare, unusual events they cannot be used to argue for or against the proposition that the *most common* Type Ia supernova is the explosion of a Chandrasekhar Mass white dwarf, only that some are.

From the factors given in Table 4, one can carry the argument farther and calculate the actual fraction of Type Ia supernova that are of this high density variety. Typical production factors for ^{48}Ca, ^{50}Ti, and ^{54}Cr are 100 relative to iron (increasing as the density increases). Timmes, Woosley, & Weaver (1995a) find that Type Ia supernovae have contributed about one-half of the iron in the sun (a reasonable range is 1/3 to 2/3). Thus Chandrasekhar Mass supernovae igniting in the density range $\rho_9 \approx 5$ to 8 should happen $\sim$2% as frequently as the common Type Ia event. This implies an interval about 50 times that of Type Ia supernovae, or roughly once every 10,000 years.

If one makes the questionable assumption that the number of white dwarfs igniting at densities greater than $\rho_9 = 8$ is comparable to the number between 5 and 8, this implies a rate for accretion induced collapse also of order 10^4 years, consistent with that required to make millisecond pulsars in our Galaxy (Bailyn & Grindlay 1990). It should be emphasized, however, that only carbon-oxygen white dwarfs are expected to produce the nucleosynthesis studied here. Neon-oxygen white dwarfs are not thought to explode, but always collapse.

^{48}Ca will not be made in any of these models if they experience prompt detonation. Detonation at the stellar center is physically unlikely (Niemeyer & Woosley 1996), but should it occur, the density separating accretion induced collapse from explosion would be raised and one would have to explore models having much higher density than 8×10^9 g cm^{-3}. Such models would need to be calculated with at least post-Newtonian approximations to general relativity.

In addition to ^{48}Ca, ^{50}Ti, ^{54}Cr, and ^{70}Zn, amounts of ^{58}Fe, ^{64}Ni, ^{66}Zn, ^{76}Ge, and ^{82}Se are produced that are of interest to Galactic chemical evolution. A test can be made of these predictions, in that the same models also produce a long-lived candidate for gamma-astronomy, ^{60}Fe ($\tau_{1/2} = 1.5 \times 10^6$ yr). Unfortunate, at least in our attempt to understand Type Ia supernovae, is the fact that Type II supernovae also make a lot of ^{60}Fe. Timmes et al. (1995b) estimate a signal from Type II's that would be about 15% of what has already observed for ^{26}Al. A signal of this strength should be detectable in the near future. The signal from the models calculated here needs to be determined from a chemical evolution calculation, but should not be too different from the roughly 20% of the total ^{60}Fe signal estimated by Timmes et al. However, the ^{60}Fe *per event* is typically 100 times greater in a high density white dwarf explosion than in a Type II supernova. With an event rate $\sim 10^{-4}$ yr^{-1}, the composite signal here comes from $\sim$100 point sources. A single source at 10 kpc that made 0.005 M$_\odot$ of ^{60}Fe would be visible for several million years at a flux level of $\sim 10^{-7}$ cm^{-2} s^{-1}. This is well beyond the capability of today's telescopes, but perhaps not out of the question in the next century, and perhaps there has been a closer event. More realistically, the signal might be distinguishable from Type II supernovae by its different Galactic distribution.

The neutron-rich nucleosynthesis is made in the deepest layers of the supernova in a place that subsequently has the lowest ejection velocity and the highest density. It is also a region devoid of ^{56}Ni and other radioactivities that might keep the gas hot and is less subject to mixing than either Type II supernovae or the layers farther out in Type Ia supernovae. All these are favorable conditions for making solid condensates. For those wishing to calculate the chemistry, the expansion speed at the edge of the 0.03 M$_\odot$ given in Table 3 at 10 s is typically 2000 km s^{-1}, the density is 2000 g cm^{-3} and the temperature 3×10^7 K. Adiabatic expansion should then lead to condensates starting to form after a few days. Back-lighting by gamma-rays from ^{56}Ni decay farther out might keep the gas warmer for a time, but it seems at least as good a place to make dust as SN 1987A.

Condensates in this region of the star would have an unusual chemical character since there is no hydrogen, carbon, oxygen, or silicon. Some of the zones of interest are more than 50% calcium. This might produce a condensate that would later be chemically reactive. Should large condensates form, the heating by ^{60}Fe could be appreciable.

It is interesting that anomalies in the isotopic composition of certain samples of the meteorite Allende have been found that show correlated excesses of ^{48}Ca, ^{50}Ti, ^{54}Cr, ^{58}Fe, and ^{66}Zn (Völkening & Papanastassiou 1990). These certainly are the characteristics of the neutron-rich nucleosynthesis studied here and their presence in a meteorite suggests a solid intermediary. Based upon Tables 3 and 4 one might also anticipate excesses of ^{64}Ni as well. A search for ^{72}Ge excesses, if feasible, would also be interesting. The lack of a ^{70}Zn excess in these samples suggests that they originate from white dwarfs that ignited between $\rho_9 = 4$ and 6. The status of Ge might clarify this.

The author appreciates the assistance of Rob Hoffman with the nuclear reaction network and preparation of the tables. He is also grateful to Tom Weaver for the use of the KEPLER stellar evolution code. This work was supported by the NSF (AST 94-17161) and, in Munich, by an award from the Humboldt Foundation.

TABLE 1

NUCLEAR REACTION NETWORK EMPLOYED (421 ISOTOPES)

Element	A_{min}	A_{max}	Element	A_{min}	A_{max}	Element	A_{min}	A_{max}
H	1	3	P	29	34	Ni	56	71
He	3	4	S	31	38	Cu	57	73
Li	6	8	Cl	34	43	Zn	60	75
Be	7	9	Ar	36	46	Ga	61	77
B	8	11	K	39	47	Ge	64	80
C	11	14	Ca	40	52	As	66	83
N	13	15	Sc	42	53	Se	68	86
O	15	18	Ti	44	54	Br	70	89
F	17	20	V	46	55	Kr	72	90
Ne	19	23	Cr	48	58	Rb	77	93
Na	21	25	Mn	50	59	Sr	79	94
Mg	23	28	Fe	52	66	Y	81	97
Al	25	30	Co	55	67	Zr	83	98
Si	27	32						
Alternate n-Rich Network (442 isotopes)								
H	1	3	P	29	34	Ni	56	72
He	3	4	S	31	38	Cu	57	73
Li	6	8	Cl	34	43	Zn	60	76
Be	7	9	Ar	36	48	Ga	61	79
B	8	11	K	39	49	Ge	64	82
C	11	14	Ca	40	54	As	67	85
N	13	15	Sc	43	55	Se	68	88
O	15	18	Ti	44	56	Br	71	89
F	17	20	V	47	57	Kr	72	90
Ne	19	23	Cr	48	58	Rb	77	93
Na	21	25	Mn	51	63	Sr	79	94
Mg	23	28	Fe	52	66	Y	81	97
Al	25	30	Co	55	67	Zr	83	98
Si	27	32						

TABLE 2
CHARACTERISTICS OF THE MODELS

Name	$\rho_{\mathrm{ign}}^{a}/10^9$g cm^{-3}	$D_{\max}$	Y_{ef}	KE$_\infty/10^{51}$ erg	M(^{56}Ni)/M$_\odot$	M(CO)^b/M$_\odot$
NCD2A	2.0	2.45	0.446	0.48	0.36	0.76
NCD2B	2.0	2.55	0.447	1.75	1.04	0.020
NCD4A	4.0	2.45	0.425	0.63	0.38	0.69
NCD4B	4.0	2.55	0.425	1.78	0.95	0.020
NCD6A	5.8	2.45	0.414	0.77	0.39	0.61
NCD6B	5.8	2.55	0.414	1.77	0.88	0.021
NCD7A	7.4	2.45	0.407	0.87	0.40	0.54
NCD7B	7.4	2.55	0.407	1.74	0.82	0.016
NCD8A	8.2	2.45	0.404	0.92	0.40	0.51
NCD8B	8.2	2.55	0.404	1.73	0.79	0.016
NCD8D	8.2	det.	0.441	2.00	0.47	···

[a]Density in central zone at the time it first reaches 2×10^9 K.

[b]Sum of the masses of unburned ^{12}C and ^{16}O in the ejecta.

Table 3
Final composition[a] of inner 0.03 $M_\odot$ (42 zones)

Isotope	NCD2A	NCD4A	NCD6A	NCD7A	NCD8A
^{48}Ca		3.1(-4)	4.6(-3)	1.6(-2)	1.8(-2)
^{49}Ca				1.4(-4)	3.7(-4)
^{50}Ca				5.4(-4)	2.4(-3)
^{49}Sc			3.9(-4)	4.2(-4)	2.0(-4)
^{51}Sc					1.5(-4)
^{50}Ti		2.3(-3)	5.1(-3)	1.3(-3)	1.5(-4)
^{51}Ti			1.6(-4)	1.3(-4)	
^{52}Ti			7.2(-4)	1.4(-3)	9.7(-4)
^{53}V			2.0(-4)	1.1(-4)	
^{55}V					1.2(-4)
^{52}Cr	8.3(-4)	1.5(-3)			
^{53}Cr		1.7(-4)			
^{54}Cr	4.0(-4)	6.1(-3)	4.8(-3)	3.4(-4)	
^{56}Cr		1.1(-4)	8.0(-4)	8.3(-4)	3.4(-4)
^{55}Mn	1.7(-4)	7.0(-4)			
^{57}Mn			1.4(-4)		
^{54}Fe	4.2(-3)				
^{55}Fe	6.9(-4)				
^{56}Fe	1.7(-2)	5.2(-3)			
^{57}Fe	1.0(-4)	2.5(-4)			
^{58}Fe	1.4(-3)	9.4(-3)	1.5(-3)		
^{60}Fe		1.2(-3)	4.2(-3)	1.2(-3)	1.8(-4)
^{62}Fe			5.5(-4)	9.9(-4)	7.4(-4)
^{57}Co	4.0(-4)				
^{59}Co		1.1(-4)			
^{58}Ni	2.6(-3)				
^{59}Ni	1.4(-4)				
^{60}Ni	3.7(-3)	1.3(-4)			
^{62}Ni	7.8(-4)	2.4(-3)			
^{64}Ni		1.4(-3)	2.5(-3)	1.1(-4)	
^{66}Ni		9.1(-4)	5.9(-3)	4.8(-3)	1.9(-3)
^{68}Ni			7.3(-4)	2.2(-3)	2.7(-3)
^{70}Ni				8.6(-4)	1.8(-3)
^{74}Zn				1.2(-4)	1.6(-4)
^{76}Zn				3.3(-4)	8.2(-4)
^{80}Ge				2.3(-4)	3.3(-4)
^{82}Ge				1.0(-4)	2.7(-4)
^{84}Se					1.6(-4)

Table 4A

Production Factors[a] for Slow Deflagrations

Isotope	NCD2A	NCD4A	NCD6A	NCD7A	NCD8A
^{12}C	.38	.30	.25	.21	.20
^{16}O	.13	.10	.08	.07	.07
^{28}Si	.19	.14	.13	.12	.12
^{32}S	.14	.12	.11	.10	.09
^{36}Ar	.15	.15	.12	.10	.10
^{40}Ca	.19	.20	.16	.13	.13
^{48}Ca	···	6.05	84.50	322.00	453.00
^{48}Ti	.16	.14	.13	.12	.12
^{49}Ti	.01	1.02	6.10	14.30	20.10
^{50}Ti	.77	37.80	106.00	165.00	214.00
^{50}V	.01	.05	.08	.09	.10
^{51}V	.14	.93	2.30	3.81	4.79
^{50}Cr	.16	.20	.21	.22	.22
^{52}Cr	.70	1.01	1.35	1.57	1.66
^{53}Cr	.53	.97	1.46	1.78	1.94
^{54}Cr	2.81	39.20	79.60	101.00	111.00
^{55}Mn	.89	1.20	1.42	1.55	1.61
^{54}Fe	2.07	2.33	2.49	2.61	2.67
^{56}Fe	1.00	1.00	1.00	1.00	1.00
^{57}Fe	1.21	1.28	1.34	1.38	1.41
^{58}Fe	1.13	7.79	13.30	15.60	16.70
^{59}Co	.52	.84	1.06	1.20	1.27
^{58}Ni	3.62	3.97	4.20	4.41	4.52
^{60}Ni	1.42	2.14	2.84	3.33	3.56
^{61}Ni	.54	.86	1.14	1.30	1.38
^{62}Ni	1.14	3.97	6.49	7.83	8.47
^{64}Ni	.04	5.31	12.80	17.50	19.50
^{63}Cu	.01	.10	.38	.60	.69
^{65}Cu	···	.08	.30	.49	.58
^{64}Zn	.14	.15	.15	.15	.14
^{66}Zn	.01	4.22	25.70	42.50	50.30
^{67}Zn	···	.12	.67	1.48	1.99
^{68}Zn	···	.05	4.65	13.90	18.40
^{70}Zn	···	.13	1.46	161.00	326.00
^{69}Ga	···	.02	.70	1.83	2.40
^{71}Ga	···	···	.16	1.55	2.34
^{72}Ge	···	.02	.51	1.19	2.41
^{73}Ge	···	···	.01	2.99	6.57
^{74}Ge	···	···	.59	3.54	4.88
^{76}Ge	···	.02	.16	48.80	118.00
^{75}As	···	···	.06	.16	.22
^{77}Se	···	···	.21	1.97	3.28
^{78}Se	···	.01	1.63	2.44	3.15
^{80}Se	···	···	1.72	9.01	13.10
^{82}Se	···	···	.04	22.50	60.00

TABLE 4A—*Continued*

Isotope	NCD2A	NCD4A	NCD6A	NCD7A	NCD8A
^{79}Br	...	...	.03	4.44	10.90
^{81}Br	...	...	.06	.26	.41
^{83}Kr	...	...	.09	2.14	4.71
^{84}Kr	...	...	.52	4.30	7.08
^{85}Rb	...	...	.07	.21	.30

[a]Production factor defined as the ratio of the production in the supernova to the given abundance in the sun normalized to unit production of ^{56}Fe. Factors that are everywhere less than 0.1 have been omitted.

Table 4B

Production Factors for Fast Deflagrations and Detonations

Isotope	NCD2B	NCD4B	NCD6B	NCD7B	NCD8B	NCD8D
^{46}Ca	···	.01	.02	.48	3.83	.03
^{48}Ca	···	2.08	36.30	157.00	230.00	.08
^{49}Ti	···	.35	2.62	7.15	10.60	.15
^{50}Ti	.13	13.20	46.70	83.30	116.00	43.90
^{51}V	.04	.37	1.08	1.98	2.60	2.49
^{50}Cr	.08	.11	.14	.15	.15	.36
^{52}Cr	.12	.32	.55	.72	.81	1.75
^{53}Cr	.22	.48	.79	1.03	1.15	2.21
^{54}Cr	.53	14.50	36.70	52.00	59.50	92.60
^{55}Mn	.48	.76	.96	1.09	1.17	2.80
^{54}Fe	1.08	1.51	1.76	1.95	2.04	4.53
^{56}Fe	1.00	1.00	1.00	1.00	1.00	1.00
^{57}Fe	1.07	1.19	1.28	1.35	1.39	2.18
^{58}Fe	.23	3.09	6.50	8.43	9.41	24.60
^{59}Co	.29	.53	.73	.86	.93	2.51
^{58}Ni	2.49	3.12	3.57	3.88	4.08	8.71
^{60}Ni	1.31	1.76	2.19	2.56	2.73	4.90
^{61}Ni	.84	.97	1.09	1.21	1.26	1.88
^{62}Ni	.53	1.96	3.58	4.60	5.16	14.10
^{64}Ni	.01	1.85	5.74	8.90	10.30	6.53
^{63}Cu	···	.04	.17	.30	.37	.16
^{65}Cu	.01	.03	.14	.25	.31	.07
^{64}Zn	.39	.36	.31	.29	.29	.14
^{66}Zn	.02	1.44	10.90	20.50	25.50	.34
^{67}Zn	···	.04	.30	.75	1.05	.06
^{68}Zn	.01	.02	2.12	6.75	9.32	.01
^{70}Zn	···	.05	.87	91.50	182.00	.04
^{69}Ga	···	.01	.28	.84	1.14	···
^{71}Ga	···	···	.08	.72	1.16	···
^{72}Ge	···	.01	.23	.68	1.64	···
^{73}Ge	···	···	.01	1.56	3.40	···
^{74}Ge	···	···	.31	1.73	2.47	···
^{76}Ge	···	.01	.07	29.10	68.40	···
^{75}As	···	···	.03	.08	.11	···
^{77}Se	···	···	.11	.98	1.67	···
^{78}Se	···	···	.74	1.20	1.62	···
^{80}Se	···	···	.94	4.43	6.58	···
^{82}Se	···	···	.02	13.80	34.90	···
^{79}Br	···	···	.01	2.51	5.95	···
^{81}Br	···	···	.03	.12	.20	···
^{83}Kr	···	···	.05	1.12	2.43	···
^{84}Kr	···	···	.28	2.21	3.64	···
^{85}Rb	···	···	.04	.10	.15	···

Table 5A

Ejected Masses^a for Slow Deflagrations

Isotope	NCD2A	NCD4A	NCD6A	NCD7A	NCD8A
^{4}He	2.19E-03	2.58E-03	2.79E-03	2.89E-03	2.85E-03
^{12}C	3.75E-01	3.36E-01	2.95E-01	2.61E-01	2.42E-01
^{16}O	4.02E-01	3.55E-01	3.13E-01	2.81E-01	2.64E-01
^{24}Mg	3.80E-03	2.87E-03	2.85E-03	2.67E-03	3.05E-03
^{27}Al	7.58E-06	3.20E-06	3.90E-06	4.28E-06	6.14E-06
^{28}Si	4.00E-02	3.37E-02	3.32E-02	3.19E-02	3.21E-02
^{29}Si	5.23E-05	5.89E-05	6.26E-05	6.07E-05	5.63E-05
^{30}Si	3.49E-06	2.33E-06	2.12E-06	2.50E-06	2.91E-06
^{31}P	1.41E-05	1.15E-05	1.19E-05	1.19E-05	1.15E-05
^{32}S	1.79E-02	1.81E-02	1.73E-02	1.54E-02	1.45E-02
^{33}S	9.46E-06	3.40E-06	3.98E-06	6.10E-06	7.27E-06
^{36}Ar	3.68E-03	4.15E-03	3.78E-03	3.22E-03	3.16E-03
^{40}Ca	3.71E-03	4.30E-03	3.77E-03	3.22E-03	3.23E-03
^{44}Ca	6.53E-06	7.84E-06	7.76E-06	7.38E-06	7.78E-06
^{46}Ca	3.50E-10	1.99E-08	5.77E-08	6.36E-07	4.91E-06
^{48}Ca	1.19E-09	3.07E-04	4.57E-03	1.80E-02	2.56E-02
^{47}Ti	4.38E-09	3.08E-08	1.29E-07	1.70E-06	7.51E-06
^{48}Ti	1.14E-04	1.07E-04	1.09E-04	1.09E-04	1.01E-04
^{49}Ti	5.14E-07	6.15E-05	3.92E-04	9.46E-04	1.35E-03
^{50}Ti	4.14E-05	2.28E-03	6.81E-03	1.10E-02	1.43E-02
^{51}V	1.66E-05	1.29E-04	3.40E-04	5.81E-04	7.40E-04
^{50}Cr	3.97E-05	5.32E-05	6.15E-05	6.54E-05	6.77E-05
^{52}Cr	3.42E-03	5.54E-03	7.87E-03	9.48E-03	1.01E-02
^{53}Cr	2.96E-04	6.15E-04	9.82E-04	1.24E-03	1.36E-03
^{54}Cr	4.00E-04	6.28E-03	1.36E-02	1.78E-02	1.98E-02
^{55}Mn	3.85E-03	5.89E-03	7.38E-03	8.33E-03	8.78E-03
^{54}Fe	4.81E-02	6.12E-02	6.96E-02	7.53E-02	7.79E-02
^{56}Fe	3.81E-01	4.30E-01	4.59E-01	4.73E-01	4.79E-01
^{57}Fe	1.13E-02	1.34E-02	1.50E-02	1.60E-02	1.64E-02
^{58}Fe	1.36E-03	1.06E-02	1.93E-02	2.33E-02	2.53E-02
^{59}Co	5.68E-04	1.03E-03	1.39E-03	1.63E-03	1.74E-03
^{58}Ni	5.84E-02	7.22E-02	8.13E-02	8.81E-02	9.15E-02
^{60}Ni	9.07E-03	1.55E-02	2.18E-02	2.64E-02	2.86E-02
^{61}Ni	1.50E-04	2.71E-04	3.84E-04	4.53E-04	4.84E-04
^{62}Ni	1.03E-03	4.06E-03	7.07E-03	8.81E-03	9.64E-03
^{64}Ni	8.94E-06	1.42E-03	3.65E-03	5.13E-03	5.79E-03
^{63}Cu	1.21E-06	2.20E-05	8.61E-05	1.39E-04	1.64E-04
^{65}Cu	3.96E-07	7.55E-06	3.15E-05	5.30E-05	6.33E-05
^{64}Zn	4.55E-05	5.34E-05	5.68E-05	5.90E-05	5.74E-05
^{66}Zn	2.78E-06	9.14E-04	5.92E-03	1.01E-02	1.21E-02
^{67}Zn	2.31E-09	3.70E-06	2.32E-05	5.25E-05	7.13E-05
^{68}Zn	1.52E-07	7.72E-06	7.39E-04	2.28E-03	3.05E-03
^{70}Zn	5.83E-11	6.79E-07	7.89E-06	9.01E-04	1.84E-03
^{69}Ga	6.45E-10	3.29E-07	1.09E-05	2.93E-05	3.89E-05
^{71}Ga	9.90E-12	2.18E-09	1.71E-06	1.70E-05	2.59E-05

TABLE 5A—*Continued*

Isotope	NCD2A	NCD4A	NCD6A	NCD7A	NCD8A
^{72}Ge	1.39E-09	3.35E-07	1.19E-05	2.86E-05	5.87E-05
^{73}Ge	1.37E-11	3.04E-09	5.37E-08	2.07E-05	4.60E-05
^{74}Ge	5.38E-12	1.31E-08	1.89E-05	1.16E-04	1.62E-04
^{76}Ge	3.86E-13	1.45E-07	1.12E-06	3.51E-04	8.63E-04
^{75}As	4.88E-14	8.28E-09	3.00E-07	8.15E-07	1.11E-06
^{77}Se	7.45E-14	1.73E-09	7.37E-07	7.29E-06	1.23E-05
^{78}Se	1.07E-13	1.24E-07	1.85E-05	2.86E-05	3.74E-05
^{80}Se	2.38E-13	3.35E-09	4.22E-05	2.28E-04	3.35E-04
^{82}Se	2.25E-14	9.14E-09	1.76E-07	1.08E-04	2.90E-04
^{79}Br	2.72E-15	1.73E-10	1.25E-07	2.16E-05	5.37E-05
^{81}Br	2.24E-15	4.52E-10	2.93E-07	1.26E-06	2.01E-06
^{83}Kr	7.03E-15	9.51E-11	3.92E-07	9.34E-06	2.08E-05
^{84}Kr	7.30E-14	4.76E-09	1.11E-05	9.50E-05	1.58E-04
^{85}Rb	2.88E-15	1.41E-09	3.11E-07	9.15E-07	1.34E-06
^{53}Mn^{b}	1.14E-04	2.01E-04	2.52E-04	2.85E-04	3.04E-04
^{60}Fe^{b}	4.95E-07	1.22E-03	4.43E-03	6.94E-03	8.04E-03
^{59}Ni^{b}	4.26E-04	6.70E-04	8.19E-04	9.36E-04	9.90E-04

[a]Ejected masses for each model in solar masses after all radioactivities have decayed. Only those isotopes for which over 10^{-6}M$_{\odot}$ is ejected are listed.

[b]Long lived radioactive nucleus.

Table 5B

Ejected Masses for Fast Deflagrations and Detonations

Isotope	NCD2B	NCD4B	NCD6B	NCD7B	NCD8B	NCD8D
^{1}H	1.95E-06	2.32E-06	1.50E-06	1.14E-06	9.82E-07	7.63E-07
^{4}He	1.50E-02	1.41E-02	1.14E-02	1.02E-02	9.62E-03	4.74E-03
^{12}C	3.30E-04	7.97E-06	8.28E-03	7.95E-03	7.88E-03	7.71E-07
^{16}O	2.07E-02	2.01E-02	1.32E-02	8.94E-03	8.16E-03	3.09E-07
^{20}Ne	2.04E-03	1.55E-06	1.52E-04	8.01E-05	2.37E-05	6.28E-08
^{23}Na	7.60E-06	2.08E-07	1.31E-06	9.64E-07	7.02E-07	1.08E-11
^{24}Mg	4.90E-03	2.92E-03	5.54E-05	4.53E-06	1.31E-06	1.54E-07
^{25}Mg	1.46E-06	1.23E-06	8.90E-07	8.08E-07	7.51E-07	1.05E-07
^{26}Mg	4.11E-06	2.68E-08	2.90E-08	1.94E-08	8.14E-09	4.49E-11
^{27}Al	2.56E-05	5.42E-06	3.21E-07	8.04E-08	4.06E-08	1.83E-09
^{28}Si	1.35E-02	1.38E-02	7.05E-03	7.80E-03	7.21E-03	2.85E-03
^{29}Si	4.93E-05	3.44E-05	2.45E-05	3.52E-05	3.24E-05	3.29E-06
^{30}Si	2.85E-06	2.63E-06	6.16E-07	6.49E-08	6.72E-08	8.82E-09
^{31}P	9.64E-06	7.70E-06	2.68E-06	1.70E-06	1.35E-06	3.11E-07
^{32}S	3.53E-03	2.90E-03	2.37E-03	4.22E-03	4.69E-03	1.79E-03
^{33}S	4.03E-06	7.51E-06	1.17E-06	2.11E-07	8.01E-10	1.08E-09
^{36}Ar	8.09E-04	5.85E-04	5.75E-04	8.45E-04	1.06E-03	3.76E-04
^{40}Ca	8.89E-04	6.85E-04	6.99E-04	7.71E-04	9.78E-04	3.12E-04
^{44}Ca	3.81E-05	3.30E-05	2.38E-05	2.01E-05	1.92E-05	6.35E-06
^{46}Ca	1.53E-10	1.63E-08	5.01E-08	1.05E-06	8.05E-06	5.12E-08
^{48}Ca	2.04E-10	2.47E-04	4.11E-03	1.69E-02	2.39E-02	6.42E-06
^{47}Ti	1.08E-08	3.35E-08	1.19E-07	2.31E-06	9.92E-06	3.75E-08
^{48}Ti	9.91E-05	8.78E-05	7.40E-05	6.24E-05	5.65E-05	1.80E-05
^{49}Ti	6.10E-07	4.98E-05	3.52E-04	9.12E-04	1.32E-03	1.43E-05
^{50}Ti	1.96E-05	1.86E-03	6.28E-03	1.06E-02	1.44E-02	4.28E-03
^{51}V	1.33E-05	1.21E-04	3.33E-04	5.80E-04	7.39E-04	5.57E-04
^{50}Cr	5.07E-05	7.29E-05	8.20E-05	8.58E-05	8.70E-05	1.58E-04
^{52}Cr	1.65E-03	4.07E-03	6.68E-03	8.38E-03	9.08E-03	1.55E-02
^{53}Cr	3.36E-04	7.06E-04	1.11E-03	1.38E-03	1.50E-03	2.26E-03
^{54}Cr	2.09E-04	5.45E-03	1.31E-02	1.76E-02	1.96E-02	2.40E-02
^{55}Mn	5.76E-03	8.65E-03	1.05E-02	1.13E-02	1.17E-02	2.22E-02
^{54}Fe	6.97E-02	9.26E-02	1.03E-01	1.08E-01	1.10E-01	1.92E-01
^{56}Fe	1.06E+00	1.01E+00	9.59E-01	9.10E-01	8.83E-01	6.95E-01
^{57}Fe	2.78E-02	2.92E-02	2.98E-02	2.99E-02	2.98E-02	3.69E-02
^{58}Fe	7.87E-04	9.86E-03	1.97E-02	2.42E-02	2.63E-02	5.41E-02
^{59}Co	8.94E-04	1.54E-03	2.01E-03	2.24E-03	2.36E-03	5.00E-03
^{58}Ni	1.11E-01	1.33E-01	1.44E-01	1.49E-01	1.52E-01	2.56E-01
^{60}Ni	2.33E-02	2.97E-02	3.52E-02	3.90E-02	4.04E-02	5.71E-02
^{61}Ni	6.54E-04	7.16E-04	7.71E-04	8.08E-04	8.17E-04	9.59E-04
^{62}Ni	1.33E-03	4.71E-03	8.16E-03	9.95E-03	1.08E-02	2.33E-02
^{64}Ni	3.84E-06	1.16E-03	3.42E-03	5.03E-03	5.68E-03	2.82E-03
^{63}Cu	1.94E-06	2.06E-05	8.25E-05	1.37E-04	1.61E-04	5.45E-05
^{65}Cu	1.66E-06	7.61E-06	3.04E-05	5.20E-05	6.27E-05	1.06E-05
^{64}Zn	3.49E-04	3.09E-04	2.53E-04	2.28E-04	2.14E-04	7.95E-05
^{66}Zn	1.25E-05	7.30E-04	5.25E-03	9.40E-03	1.13E-02	1.19E-04

Table 5B—*Continued*

Isotope	NCD2B	NCD4B	NCD6B	NCD7B	NCD8B	NCD8D
^{67}Zn	4.99E-08	3.13E-06	2.13E-05	5.14E-05	6.94E-05	3.36E-06
^{68}Zn	1.99E-06	8.00E-06	7.05E-04	2.13E-03	2.86E-03	1.55E-06
^{70}Zn	8.58E-12	5.67E-07	9.84E-06	9.82E-04	1.90E-03	3.13E-07
^{69}Ga	5.16E-09	2.71E-07	9.22E-06	2.59E-05	3.42E-05	1.52E-08
^{71}Ga	4.25E-10	2.48E-09	1.70E-06	1.52E-05	2.36E-05	1.41E-09
^{72}Ge	2.15E-08	3.08E-07	1.12E-05	3.12E-05	7.37E-05	6.70E-09
^{73}Ge	9.78E-11	3.23E-09	7.51E-08	2.08E-05	4.39E-05	5.78E-10
^{74}Ge	1.32E-12	1.29E-08	2.06E-05	1.09E-04	1.52E-04	8.70E-09
^{76}Ge	1.61E-14	1.30E-07	1.08E-06	4.03E-04	9.19E-04	1.45E-08
^{75}As	6.92E-13	8.89E-09	2.95E-07	7.88E-07	1.06E-06	1.65E-10
^{77}Se	1.90E-12	1.68E-09	7.99E-07	6.96E-06	1.15E-05	6.88E-11
^{78}Se	7.29E-14	1.16E-07	1.77E-05	2.71E-05	3.55E-05	2.53E-10
^{80}Se	3.37E-14	3.52E-09	4.81E-05	2.15E-04	3.10E-04	7.22E-10
^{82}Se	5.90E-16	8.09E-09	1.67E-07	1.27E-04	3.10E-04	1.37E-09
^{79}Br	1.49E-14	1.63E-10	1.29E-07	2.34E-05	5.39E-05	3.63E-11
^{81}Br	2.09E-14	4.13E-10	2.68E-07	1.13E-06	1.75E-06	2.61E-11
^{83}Kr	1.62E-15	9.09E-11	4.54E-07	9.40E-06	1.98E-05	6.01E-11
^{84}Kr	4.46E-14	4.49E-09	1.25E-05	9.37E-05	1.50E-04	5.47E-11
^{85}Rb	8.79E-16	1.30E-09	3.28E-07	8.81E-07	1.26E-06	8.16E-11
^{53}Mn	1.26E-04	2.66E-04	3.37E-04	3.76E-04	3.89E-04	8.43E-04
^{60}Fe	1.49E-07	9.66E-04	4.01E-03	6.54E-03	7.64E-03	7.00E-04
^{59}Ni	5.67E-04	9.83E-04	1.22E-03	1.36E-03	1.41E-03	3.21E-03

REFERENCES

Anders, E., & Grevesse, N. 1989, Geochim. Cosmochim. Acta, 53, 197

Aparicio, J. M., & Isern, J. 1993, å, 272, 446

Aufderheide, M., Fushiki, I., Woosley, S. E., & Hartmann, D. H. 1994, ApJS, 91, 389

Bailyn, C. D., & Grindlay, J. E. 1990, ApJ, 353, 159

Barkat, Z., & Wheeler, J. C. 1990, in Supernovae, eds. C. Wheeler, T. Piran, & S. Weinberg, Jerusalem Winter School for Theoretical Physics, Vol. 6, World Scientific, p. 111

Benz, W. 1996, in Thermonuclear Supernovae, eds. R. Canal & P. Ruiz LaPuente, in press.

Blinnikov, S., & Sasorov, P. V. 1995, Phys. Rev. E, submitted.

Blinnikov, S.I., & Khokhlov, A. 1987, Sov. Astron. Lett, 13, 364

Canal, R., Isern, J., & Labay, J. 1990. ARA&A, 28, 183

Caughlan, G. A., & Fowler, W. A. 1988, ADNDT, 40, 283

Fuller, G. M., Fowler, W. A., & Newman, M. 1980, ApJS, 42, 447

Fuller, G. M., Fowler, W. A., & Newman, M. 1982, ApJS, 48, 279

Fuller, G. M., Fowler, W. A., & Newman, M. 1985, ApJ, 293, 1

Garcia-Senz, D., 1992, in Supernovae: Menorca School of Astrophysics, eds. E. Bravo et al., Societat Catalana de Fisica, p. 161

Garcia-Senz, D., & Woosley, S. E. 1995, ApJ, 454, 895

Garcia-Senz, D., Bravo, E., & Woosley, S. E. 1996, in Thermonuclear Supernovae, eds. R. Canal & P. Ruiz LaPuente, in press.

Hartmann, D. H., Woosley, S. E., & El Eid, M. 1985, ApJ, 297, 837

Hernanz, M., & Isern, J. 1992, in Supernovae: Menorca School of Astrophysics, eds. E. Bravo et al., Societat Catalana de Fisica, p. 133

Höflich, P., & Khokhlov, A. 1996, ApJ, in press.

Iben, I. Jr. 1982, ApJ, 253, 248

Isern, J., & Canal, R. 1994, in IAU Colloq. 147: The Equation of State in Astrophysics, eds. G. Chabrier & E. Schatzman (Cambridge Univ. Press), p. 186

Khokhlov, A. 1995, ApJ, 449, 695

Meyer, B. S., Krishnan, T., & Clayton, D. D. 1996, ApJ, 462, 825

Niemeyer, J.C., & Woosley, S. E. 1996, ApJ, in press.

Nomoto, K., Thielemann, F.-K., & Yokoi, K. 1984, ApJ, 286, 644

Nomoto, K., & Kondo, Y. 1991, ApJ, 367, L19.

Nomoto, K., Iwamoto, K., & Thielemann, F.-K. 1996, BAAS, Vol. 27, No. 4, p. 1307

Rappaport, S., Di Stefano, R., & Smith, J. D. 1994, ApJ, 426, 692

Sharp, D. H. 1994, Physica D, 12, 3

Thielemann, F.-K., Nomoto, K., Iwamoto, K., & Brachwitz, F. 1996, in Proc. International Symposium on Type I Supernovae, R. Canal and P. Ruiz-LaPuente editors, in press

Timmes, F. X. 1994, ApJ, 423,L131

Timmes, F.X., & Woosley, S.E. 1992, ApJ, 396, 649

Timmes, F. X., Woosley, S. E., & Weaver, T. A. 1995a, ApJS, 98, 617

Timmes, F. X., Woosley, S. E., Hartmann, D. H., Hoffman, R. D., Weaver, T. A., & Matteucci, F. 1995b, ApJ, 449, 204

Völkening, J., & Papanastassiou, D. A., 1990, ApJ, 358, L29

Weaver. T. A., Zimmerman, G. B., & Woosley, S. E. 1978, ApJ, 225, 1021

Woosley, S. E., Fowler, W. A., Holmes, J. A., & Zimmerman, G. B. 1978, ADNDT, 22, 371

Woosley, S. E., & Weaver, T. A. 1986, in Radiation Hydrodynamics in Stars and Compact Objects, eds. D. Mihalas & K.-H. A. Winkler, (Springer Verlag:Berlin), p. 91

Woosley, S.E. 1990, in Supernovae, ed. A.G. Petschek (Berlin: Springer-Verlag), p.182

Woosley, S. E., and Eastman, R. G. 1995, Proceedings of Menorca School of Astrophysics, eds. E. Bravo, R. Canal, J. Ibanez, and J. Isern, Societat Catalana de Fisica, p. 105

Woosley, S. E., & Hoffman, R. D. 1992, ApJ, 395, 202

Woosley, S. E., Wilson, J. R., Mathews, G., Meyer, B. & Hoffman, R. 1994, ApJ, 433, 229

Woosley, S. E., & Weaver, T. A. 1994, in Supernovae, Session LIV, Les Houches, eds. S. Bludman, R. Mochovitch, and J. Zinn-Justin, Elsevier Science Publishers, p. 63.

Woosley S. E., Weaver, T. A., & Hoffman, R. D. 1995, in Proc. of 3^{rd} Intn. Symp. on Nuclei in the Cosmos, eds. M. Busso, R. Gallino, & C. Raiteri, (AIP Conf. Ser. 327), p. 463

This 2-column preprint was prepared with the AAS LaTeX macros v4.0.

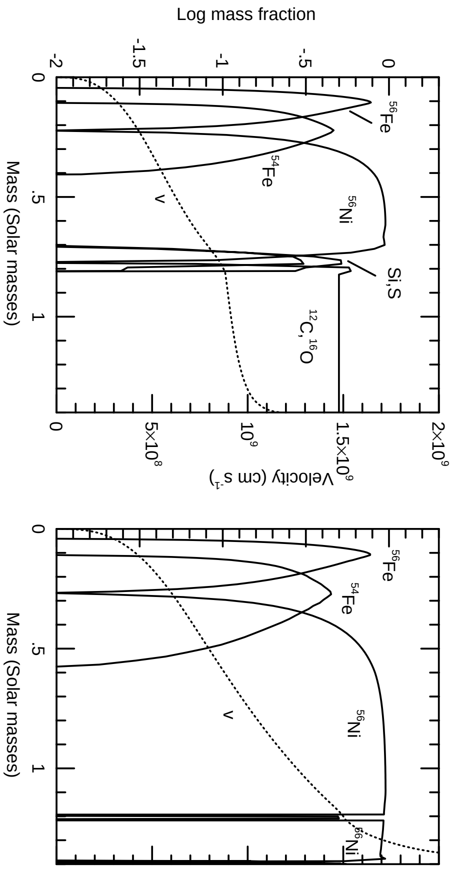

Fig. 1.— Abundances of the major isotopes, ^{56}Fe, ^{54}Fe, ^{56}Ni, ^{32}S, ^{28}Si, and ^{16}O in the final ejecta of Models NCD6A (left) and NCD6B (right). Also given as a dashed line in each figure is the final velocity (evaluated at 10 seconds) of the explosion.

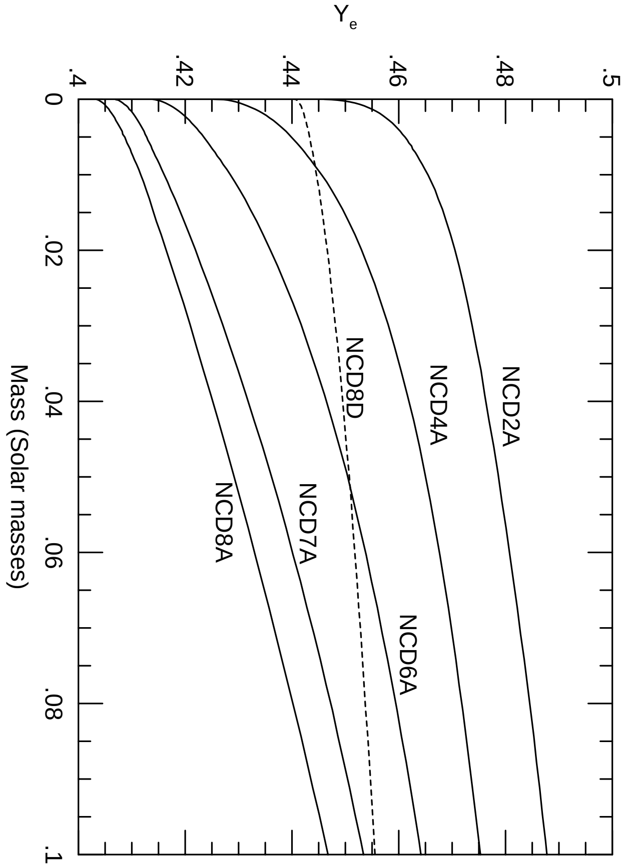

Fig. 2.— Distribution of the final value of Y_e in the inner 0.1 M$_\odot$ of the lower energy versions of each model plus the prompt detonation Model NCD8D.